

DOI: 10.1002/ ((please add manuscript number))

Article type: Full Paper

Surface functionalization of metal–organic frameworks through direct metal-coordination with a phenolic lipid enables diverse applications

Wei Zhu,^{a,b} Guolei Xiang,^c Jin Shang,^d Jimin Guo,^b Benyamin Motevalli,^e Paul Durfee,^b Jacob Ongudi Agola,^b Eric N. Coker,^a and C. Jeffrey Brinker,^{a,b,}*

Dr. W. Zhu, E. N. Coker, and Prof. C. J. Brinker
Advanced Materials Laboratory, Sandia National Laboratories, Albuquerque, New Mexico
87185, USA
E-mail: cjbrink@sandia.gov

Dr. W. Zhu, J. Guo, P. Durfee, J. O. Agola, and Prof. C. J. Brinker
Center for Micro-Engineered Materials and the Department of Chemical and Biological
Engineering, The University of New Mexico, Albuquerque, New Mexico 87131, USA

Dr. G. Xiang,
Melville Laboratory for Polymer Synthesis, Department of Chemistry, University of
Cambridge, Lensfield Road, Cambridge CB2 1EW, United Kingdom

Dr. J. Shang,
Joint Laboratory for Energy and Environmental Catalysis, School of Energy and Environment,
City University of Hong Kong, Tat Chee Avenue, Kowloon, Hong Kong SAR, P. R. China

Dr. B. Motevalli,
Department of Mechanical and Aerospace Engineering, Monash University, Clayton, Victoria
3800, Australia

Keywords: metal-organic framework, surface functionalization, metal-phenolic coordination, interfacial assembly, bioapplication

A novel strategy for the versatile functionalization of the external surface of metal-organic frameworks (MOFs) has been developed based on the direct coordination of the phenolic-inspired lipid molecule DPGG (1,2-dipalmitoyl-sn-glycero-3-galloyl) with the metal nodes uniformly distributed on the MOF external surface. XRD and Argon (Ar) sorption analysis prove that the modified MOF particles retain their structural integrity and porosity after surface modification. Density functional theory (DFT) calculations also reveal that strong chelation strength between the metal nodes and the galloyl head group of DPGG is the basic

prerequisite for successful surface coating. Due to the pH-responsive nature of metal-phenol complexation, the modification process is completely reversible by simple washing in weak acidic water, showing an excellent regeneration ability. Moreover, the colloidal stability of the modified MOF particles in the nonpolar solvent, toluene, allows them to be further organized into 2D MOF or MOF/polymer monolayer arrays by evaporation-induced interfacial assembly conducted on an air/water interface. Finally, the facile assembly of a second functional layer onto DPGG-modified MOF cores, enabled a series of MOF-based functional nanoarchitectures, such as MOF-based hybrid supported lipid bilayers (*protocells*), polyhedral core-shell structures, plasmonic vesicles, and multicomponent nanocarriers with target functionalities, to be generated for a wide range of applications.

1. Introduction

Due to their chemical diversity, tunable porosity, and high surface areas, metal–organic frameworks (MOFs) have gained tremendous interest for a wide range of applications including gas storage, chemical catalysis, light harvesting, sensing, and drug delivery.^[1] Given their highly modular nature, the introduction of additional/multiple functional groups into MOF architectures has the potential to further enrich the functional diversity, however, *de novo* synthesis of MOFs incorporating a target functionality (i.e., one-pot solvothermal synthesis) always encounters problems with ligand solubility/stability, and/or the formation of undesirable structures or side products.^[2] Currently, post-synthesis incorporation of desired functionalities within a given MOF system without disrupting the metal–organic linker bonds has become an important strategy to address the synthetic challenges associated with the *de novo* MOF synthesis.^[3] Through post-covalent modification with functional organic ligands or linker reactive sites or the post-grafting of co-ordinatively unsaturated metal sites (CUS) with chelating agents, MOF systems with specific functionalities, such as increased moisture

resistance and H₂ uptake through post-reaction with hydrophobic alkyl chains,^[4] biofunctionality (e.g. biocompatibility, cellular transfection capability, targeted cancer therapy, etc.) via post click chemistry,^[5] catalytic activity, selective adsorption, and molecular recognition capability via dative bonding of electron-rich functional groups on CUS of Cr or Zr-based MOFs,^[6] and the integration of fluorescence emission, photocatalytic activity, and *in vivo* imaging ability based on post-synthetic metalation,^[7] have been realized. However, until now surface functionalization of MOFs is still in its infancy, and consequently investigation and assessment of new functions of novel MOF nanoarchitectures are of increasing interest.^[8] In particular, so far only a few strategies have been developed to enable versatile MOF modification/functionalization.

Metal-phenolic coordination structures are of wide-spread interest due to the coupled benefits of metal ion-based inorganic and phenolic-based organic building blocks.^[9] Due to their fast and reversible coordination abilities, phenolic-based or inspired molecules have been used extensively as building blocks to fabricate exotic structures with advanced functionalities,^[10] such as multifunctional capsules,^[10a] hollow MOFs,^[10b] and superstructured assemblies.^[10d] Inspired by this well-defined coordination chemistry, we here present a novel strategy for the versatile functionalization of the MOF outer-layer surface based on simple coordination with the phenolic-based lipid molecule DPGG by a phase transfer process (Figure 1A and Figure S1). The key point is the strong coordination interactions between the activated metal-binding sites surrounding the MOF surface and the galloyl head group of DPGG, which enables easy and rapid surface coating within 5 minutes without disrupting the MOF structural integrity and porosity. As a demonstration, a variety of metal ion (Zn²⁺, Co²⁺, Zr⁴⁺, Fe³⁺, Cu²⁺, Cr³⁺, Mn²⁺, In³⁺, Al³⁺, and Eu³⁺)-based MOFs, have been synthesized and used to prove the general coating capability. DFT calculations reveal that a strong chelating ability is the basic prerequisite for the successful modification. Interestingly, due to the pH-responsive nature of metal-phenol complexation, the modification process can be completely

reversed by simple washing in weak acidic water, allowing MOF regeneration for real- world applications. Moreover, owing to the organic solvent compatibility of modified MOFs, directional interfacial self-assembly of colloidal MOF particles or MOF particle/polymer monolayers at an air/water interface could also be easily achieved. Additionally, through fusion of a second functional layer such as a targeting lipid, an amphiphilic methoxysilane, gold nanoparticles (NPs), hydrophobic mesoporous silica NPs, or small MOF NPs with different porosity and pH-disassembly characteristics, onto DPGG-modified MOF cores, diverse MOF-based functional materials (MOF-based hybrid *protocells*, polyhedral core-shell structures, plasmonic vesicles, and multicomponent nano carriers) with target functionalities could also be efficiently generated for an array of potential applications, including drug delivery, targeted cancer therapy, photothermal therapy, etc. Taken together, we believe our novel and versatile coating strategy will greatly promote the design of new MOF-inspired nanoarchitectures for a wide range of applications.

2. Results and Discussion

The surface functionalization of MOF particles by the lipid-analogue molecule DPGG was carried out by a phase transfer process (Figure 1A). In a typical synthesis, the MOF nanoparticles dispersed in water solution (1 mg/mL) were directly added to a chloroform solution of DPGG (1 mg/mL). After vortexing the suspension for several minutes, ethanol was added to break the emulsion, and the DPGG-modified MOF particles were collected by centrifugation, washed with ethanol, and dried under vacuum. To prove the successful modification, UiO66 MOF particles, composed of $Zr_6O_4(OH)_4$ octahedral metal nodes (Figure 2A) and 2,4-benzene-dicarboxylic linkers,^[11] were first synthesized and used for demonstration. As shown in Figure S2, UiO66 MOF particles have a uniform size of around 170 nm and exhibit a well-defined octahedral shape. Owing to their hydrophilicity, dispersion of UiO66 particles in the nonpolar solvent toluene causes rapid aggregation (Figure S3A).

However, after modification, the colloidal stability of UiO66 in toluene is greatly improved. After addition of DPGG-modified UiO66 particles in a toluene/water mixed solution, the surface modified nanoparticles are preferentially retained in the toluene layer (Figure S3B), consistent with the transformation of surface properties to hydrophobic. Based on DFT calculations (Figure 2B-C), the binding energy between the Zr-based metal node and the chelating fragment of DPGG was determined to be ca. 0.75 eV, indicating a strong binding affinity. We believe the strong chelation between metal sites and the galloyl group of DPGG is the basic prerequisite for the successful coating. Fourier Transform-Infrared Spectroscopy (FTIR) of the DPGG-UiO66 conjugates in Figure 2D also reveals the presence of alkane (C-H) and carbonyl (C=O) vibrational peaks at 2917 cm^{-1} and 1737 cm^{-1} , respectively, which are also present in the FTIR spectrum of free DPGG, but not in the FTIR spectrum of the unmodified MOFs. Also as shown in Figure S4, the Zr $3d_{5/2}$ X-ray photoelectron spectroscopy (XPS), UiO66 exhibits a binding energy of 183.1 eV which corresponds to the Zr(IV) oxidation state $[\text{Zr}_6\text{O}_4(\text{OH})_4(-\text{CO}_2)_{12}]$,^[12] while for modified MOFs the $3d_{5/2}$ peak shifts from 183.1 to 182.5 eV, which can be deconvoluted and fitted to two peaks assigned to $[\text{Zr}_6\text{O}_4(\text{OH})_4(-\text{CO}_2)_{12}]$ (183.1 eV), and Zr- O_{DPGG} (182.47 eV). This highlights that the Zr(IV) is coordinated by phenolic groups. Moreover, as shown in Figure 2E, powder X-ray diffraction (PXRD) confirms that the DPGG-functionalized MOF sample retains the same crystallinity as the parent UiO66. The Ar adsorption isotherm is Type I consistent with a microporous solid, and the BET surface area (S_{BET}) is calculated to be $1068.9\text{ m}^2/\text{g}$ (Figure 2F). After DPGG modification, the adsorption isotherm remains nearly unchanged, and we observe only an 8.6% drop in surface area to $976.5\text{ m}^2/\text{g}$, indicating that the modified MOF particle retains its porosity and that the modification is limited only to the external surface, as no surface area would be accessible if the MOF particles were completely modified. The transmission electron microscope (TEM) image in Figure S5 also proves no change of the particle shape or outer-surface structure occurs due to modification. All of the structural

characterization studies demonstrate the good preservation of structural integrity and porosity of MOF particles after DPGG modification.

Due to the diverse metal-chelation abilities of DPGG, our phase transfer process should also be suitable for other MOF systems. As a demonstration, 9 types of other metal (Zn^{2+} , Co^{2+} , Fe^{3+} , Cu^{2+} , Cr^{3+} , Mn^{2+} , In^{3+} , Al^{3+} , and Eu^{3+})-based MOF particles with different surface chemistries have been synthesized. Following the same modification process, DPGG-modified MOF particles with various morphologies, sizes, and compositions have also been obtained (Figure 1C). FTIR spectra in Figure S6 confirm that all the MOF particles are successfully modified with DPGG. XRD (Figure S7) and Ar sorption analyses (Table 1) further confirm that all the modified MOF particles have preserved crystallinities and permanent porosities, indicating a versatile modification approach. Additionally, as a control experiment, when the DPGG-analogue molecule gallic acid without hydrophobic alkyl chains was used instead of DPGG, only etched hollow MOF particles (ZIF-67) were obtained (Figure S8), indicating that the presence of the long hydrophobic alkyl chain is necessary to avoid the inward binding of metal sites or the replacement of inner organic linkers by DPGG. Note that MOF nanoparticle etching by gallic acid has been observed previously.^[10e] Also due to the fast transfer of MOF particles from water phase to chloroform within several minutes, the etching of any water unstable MOF architectures has been efficiently suppressed. Due to the diverse surface chemistries of MOFs, we believe that our post-synthesis modification process is varied and should be different from MOF to MOF. For the MOF systems with unsaturated metal sites such as MIL-100(Fe),^[13] the coordination of DPGG can directly occur in DPGG chloroform solution as shown in Figure S9. However, for some other MOF systems such as ZIF-8 and ZIF-67, a dense modification only occurs with the assistance of water to decrease the stability of metal-linker bonds surrounding the MOF external surface and thus promote the replacement of organic ligands by DPGG. Summarizing, the modification process in our work involves dative bonding at the unsaturated metal sites and solvent-

assisted external linker exchange, and the high binding affinity between phenol units and metal sites is the major driving force.

An important feature of metal-phenolic coordination is the pH-dependent behavior, which allows reversible modification of the MOF surface.^[9] So far, reports of reversible functionalization of MOF surfaces are still very limited but are of potentially high interest for real-world applications. In our case, for the proof of this assumption, a Fe(III)-based MOF (MIL-88A) (Figure 3A) was chosen due to its three different binding states between Fe(III) and phenol groups (pH<2: mono-, 3<pH<6: bis-, pH>7: tris-complex) (Figure 3D).^[9a] The successful modification of MIL-88A MOF particles with DPGG was proven by FTIR in Figure S5, and correspondingly by the different wetting properties (Figure 3B) and colloidal stabilities (Figure 3C) before and after modification. Note that MIL-88A was found to be hydrophilic, absorbing water droplets and displaying contact angle close to 10.6°. However, after the modification with long alkyl substituents, the contact angle was observed to be ~126.7°. Even after exposure to ambient air for several weeks, the contact angle remained the same, indicating a very stable modification. Similar to Fe(III)-phenol binding, Fe(III)-galloyl binding in our case was also pH-dependent (Figure 3E). The treatment of DPGG-modified MIL-88A sample at pH 7.4 buffer for several hours resulted in no reduction in the intensities of DPGG related vibrations in FTIR spectrum (Figure 3F). However, after washing in buffer at pH 5.0, the DPGG-related vibration intensity centered at 2950 and 1705 cm⁻¹ decreased, and even disappeared when the pH was lowered to 1.0, clearly proving the pH-dependent disassembly behavior arising due to the progressively reduced coordination of Fe(III) with decreasing pH (Figure 3D). This reversible pH-dependent surface modification characteristic should enable the recycling and utilization of water-stable MOFs, especially important for MOFs that are hard to synthesize and/or expensive.

The post-functionalization of MOFs with lipid-analogue DPGG molecules without disruption of their structural integrity imparts new functionalities and additionally enables

MOFs to be employed in other powerful fabrication strategies, such as evaporation-induced self-assembly conducted at an air/water interface to form larger scale nanoparticle arrays.^[14] Here we first hypothesized that for the DPGG-modified MOF system, the long hydrophobic chains surrounding the MOF external surface would improve the moisture/water resistance (Figure 4A). To demonstrate this concept, HKUST-1, a copper-based moisture-sensitive MOF, was chosen owing to its relatively weak metal-carboxylic coordination which enables attack by water and consequently framework decomposition.^[4] First, as shown in Figure 4B, the presence of alkane (C-H) and carbonyl (C=O) vibrational peaks at 2920 cm^{-1} and 1735 cm^{-1} , respectively, proves the DPGG modification on HKUST-1 particle surface. In Figure 4C, the framework and crystallinity of the DPGG-coated HKUST-1 remained unaltered after modification, and Ar sorption results were consistent with the parent HKUST-1 (Figure 4D) viz. the S_{BET} for pristine and coated HKUST-1 are calculated to be 1920.6 and 1823.6 m^2/g , respectively, suggesting that the intrinsic HKUST-1 porous structure was preserved. Upon the incubation of both modified and unmodified HKUST-1 nanoparticles in water for 12 h, PXRD (Figure 4C) indicates that the pristine structure of HKUST-1 has been completely changed, demonstrating major structural changes taking place. In contrast, the structure of the DPGG-modified HKUST-1 was virtually unchanged over the same period treatment time. Correspondingly, S_{BET} results show the evident decrease of the BET surface area of unmodified HKUST-1 from 1920.6 to 3.9 m^2/g , while DPGG-modified HKUST-1 only shows a more modest loss in surface area from 1823.6 to 1199.4 m^2/g . These structural studies prove unambiguously that DPGG-modification protects MOFs from water attack attributed to vulnerable metal coordination bonds, thus preserving MOF structural integrities.

Assembly of colloidal MOFs into two-dimensional (2D) and quasi-3D arrays may enable the integration of functional MOF-based building blocks into well-defined periodic structures of potential interest for metamaterials, plasmonic, photonic-based sensing and surface patterning/ templating.¹⁵ In our case, the colloidal stability of DPGG-modified MOF particles

in the non-polar solvent toluene allows rapid fabrication of MOF monolayers by evaporation-induced interfacial self-assembly.¹⁴ Here due to the easy synthesis of highly monodispersed MOF particles in methanol solution, ZIF-8 particles with rhombic dodecahedra morphology were first used as a prototypical MOF particle. The interfacial assembly of ZIF-8 particles on an air/water surface was carried out by dispensing a small droplet (30 μ L) of DPGG-modified ZIF-8 MOFs in toluene solution (30 mg/mL) onto the water surface (Figure 5A). Rapid droplet spreading and phase separation of hydrophobic MOF particles to the air/water interface followed by contact line pinning and solvent evaporation drives the self-assembly of a closed packed 2D MOF monolayer within only several seconds. As shown in Figure 5B, a monolayer of ZIF-8 MOF particles organized into a close-packed hexagonal array and $\langle 111 \rangle$ crystal orientation was obtained. Compared with MOF assembly by drop-casting and solvent drying on a solid substrate,^[15a] our MOF particle packing was more dense, due to the trapping of the hydrophobic MOFs at the fluid hydrophobic toluene/air interface allowing facile evaporation-driven assembly into close packed arrays without interference from the solid support. After toluene solvent evaporation is complete the array is transferred to the water surface as a free-standing film. Water drying then transfers the array to the solid silica surface. The dominance of the 110 and 220 reflections in the related XRD pattern (Figure 5C) further proved the oriented assembly. Moreover, for UiO66 MOF particles with well-defined octahedral shapes, a hexagonal close packing (HCP) could also be achieved by the same assembly route (Figure 5D). Unexpectedly, by soaking the ZIF-8 HCP arrays in water for several days, which caused the partial etching of ZIF-8 nanoparticle by water, an inverse structure could also be fabricated as a template for potential lithography (Figure 5E). In particular, it is also possible to assemble MOF monolayers as free-standing films supported within a polymer by performing interfacial assembly with an oil-soluble commercial polymer (poly(methylmethacrylate): PMMA) added to the toluene/MOF solution. In Figure 5F-G, DPGG-modified ZIF-8 MOF particles with cubic shape were dispersed in a PMMA polymer-

containing toluene solution and dispensed on the water interface. Hydrophobic MOFs phase separate to free solvent/air and ultimately polymer/air interface where evaporation drives their assembly into 2D arrays. It can be expected that the fast modification of MOF surfaces by DPGG without morphology change will open up a host of opportunities for the creation of novel MOF-based superassemblies.

Nanoscale MOFs, owing to their high drug loading capabilities, biodegradability, and versatile functionality, have been considered as a promising platform for drug delivery.^[16] In our case, due to the hydrophobic nature of DPGG-modified MOFs, the sequential fusion of a second functional layer provides an easy and highly controllable method to fabricate a series of water soluble, MOF-based functional nanoarchitectures for target bioapplications. As a demonstration, a suspension of lipid plus DPGG-modified colloidal MOF, ZIF-8 or MIL-88A, was prepared in 60/40 (v/v) H₂O/EtOH mixture, where the lipid exists as a monomer, was quickly added to water. After increasing the water concentration and employing sonication to promote organic solvent evaporation, the hydrophobic MOF particles were transferred into the aqueous phase by an interfacial process driven by hydrophobic van der Waals interactions between the primary long alkane chain of DPGG and the secondary alkane of the lipid, resulting in thermodynamically defined interdigitated hybrid lipid bilayer structures (referred to as *protocells*) (Figure 6, Route 1). As shown in Figure 7A, direct Cryo-TEM observation of 1,2-dioleoyl-sn-glycero-3-phospho-L-serine (DOPS)-fused DPGG-modified MIL-88A MOF particles showed evidence of a hybrid supported lipid bilayer with thickness of ~10 nm (Figure 7B), consistent with reported thickness values of vesicle bilayers.^[17] A fluorescence microscopy image of DPGG-modified ZIF-8 particles (~2 μm) after the fusion of a FITC-labeled positively charged lipid 1,2-dioleoyl-3-trimethylammonium-propane (DOTAP) also proved the formation of hybrid bilayers (Figure 7C). Compared with direct fusion of lipid-bilayer vesicles to particle surfaces such as mesoporous silica nanoparticles,^[17] our sequential lipid fusion method can overcome surface charge interaction issues and thus any lipid

(positive, negative, or neutral) can be functionalized separately from the MOF surface and incorporated into the outer leaflet of a hybrid bilayer, as shown by corresponding zeta potential measurements (Figure 7D). The outer layer leaflet can be further modified by targeting ligands and polyethylene glycol (PEG) for applications in targeted cancer therapy.^[18] To demonstrate, DPGG-functionalized MOFs (MIL-100) (Figure 8) were first fused with a lipid mixture (molar ratio, 96% 1,2-Dioleoyl-sn-glycero-3-phosphocholine (DOPC): 2% 1,2-distearoyl-sn-glycero-3-phosphoethanolamine-N-[methoxy (polyethyleneglycol)-2000] (ammonium salt) (DSPE-PEG2000): 2% 1,2-distearoyl-sn-glycero-3-phosphoethanolamine-N-[biotinyl(polyethylene glycol)-2000] (ammonium salt)) (DSPE-PEG(2000) Biotin). After the further functionalization of DSPE-PEG(2000) Biotin with NeutrAvidin as a coupling ligand, the monoclonal antibody of EGFR-biotin could be easily grafted onto the MOF outlayer surface to enable targeting. Herein, a lung cancer cell A549 (adenocarcinomic human alveolar basal epithelial cell) was used as the target cell due to the high expression of EGFR antigen on the cell outer surface. First, we tested the toxicity of bare MIL-100 NPs and MIL-100-DPGG-DOPC/DSPE-PEG2000 protocells toward A549 cells employing a CellTiter-Glo® 2.0 cell viability assay. Figure 8A shows both bare and functionalized MOFs are only moderately toxic even at high concentrations (200 µg/mL). As a proof-of-concept, the red fluorescent dye, rhodamine isothiocyanate, was loaded into the EGFR-functionalized MIL-100-based protocell as a model cargo. Then the drug-loaded protocells were incubated with A549 cells for different time intervals to evaluate the cellular internalization and targeting. The cellular filamentous actin network and nuclei were stained with fluorescent probes of Alexa Fluor 488 phalloidin and Hoechst 33342, respectively. After incubation of MOFs or protocells with A549 cells for 2 h, MOF NPs (MIL-100-DPGG-DOPC/DSPE-PEG2000) without EGFR antibody modification, showed no cellular binding or internalization by fluorescent microscopy (Fig. 8B). However, with EGFR antibody functionalization, a significant selective binding to A549 cells (Figure 8C-D) was achieved, demonstrating

targeted binding. The low toxicity and selective binding of the targeted MOF-based protocells supports their potential use for drug delivery applications. Moreover, using the same process but employing organo-silane surfactants (Figure 6, Route 2 and Figure S10) or a mixture of organo-silane and PEG-modified lipids, followed by further condensation with tetraethyl orthosilicate (TEOs), SiO₂-encapsulated colloidal MOFs (Figure 7E) or PEG-modified SiO₂-encapsulated colloidal MOFs (Figure 7F) could also be easily achieved that should exhibit good *in vivo* circulation for MOF-based drug nanocarriers.

The DPGG-modified MOF surface can also provide an excellent platform to allow the controlled superassembly of diverse functional particles on colloidal MOF surfaces, such as gold nanoparticles for the synthesis of plasmonic vesicles (Figure 7G) and their related hollow structures (Figure 7H) following etching in ethylenediaminetetraacetic acid (EDTA) supplemented buffer solution; small MOF nanoparticles with different porosity and pH-disassembly behaviors (Figure 7I); or mesoporous silica nanoparticles (Figure 7J) for the construction of multicompartiment nanocarriers. The modular assembly coupled with the ability to separately design and independently fabricate the MOF core and functional shell, opens new routes for the fabrication of exotic structures with advanced functionalities. Right now, the potential applications for drug delivery, targeted cancer therapy, and photothermal therapy, are being investigated.

3. Conclusion

In summary, based well-defined metal-phenolic coordination chemistry, a novel strategy for the versatile and reversible functionalization of the MOF external surface with the phenol-inspired lipid molecule DPGG has been developed that preserves the MOF structural integrity and porosity. On one hand, by forming essentially a self-assembled monolayer composed of long hydrophobic alkyl chains on the MOF outer-layer surface, moisture/water resistance and colloidal stability in non-polar solvents has been greatly improved. Hydrophobic MOFs can

be further assembled into 2D monolayer arrays at an air/water interface via evaporation-induced interfacial assembly. On the other hand, the sequential fusion of a second functional lipid monolayer on the DPGG-modified MOF cores results in a MOF-encapsulated within a conformal hybrid lipid bilayer that can be further modified to form MOF-based functional nano architectures such as hybrid protocells, polyhedral core-shell structures, plasmonic vesicles, and multicomponent nanocarriers with potential bioapplications (drug delivery, targeted cancer therapy, photothermal therapy, *etc.*). We believe our findings will open new avenues for artificially designed MOF-inspired functional materials for wide ranging applications.

4. Experimental Section

DPGG Modification of MOF particle surface based on phase transfer reaction: In a typical synthesis, the MOF nanoparticles dispersed in water solution (1 mg/mL) were directly added to a chloroform solution of DPGG (1 mg/mL). After vortexing the suspension for several minutes, ethanol was added to break the emulsion, and the DPGG-modified MOF particles were collected by centrifugation, washed with ethanol, and dried in vacuum.

DPGG-modified MOF particle interfacial assembly on air/water interface: The interfacial assembly of MOF particles on an air/water interface was carried out by dispensing a small droplet (30 μ L) of DPGG-modified MOFs in toluene solution (30 mg/mL) onto the water surface. Rapid droplet spreading and phase separation of hydrophobic MOF particles to the air/water interface followed by contact line pinning and solvent evaporation drives the self-assembly of a closed packed 2D MOF monolayer within only several seconds.

Lipid fusion onto DPGG-modified MOF particle surface: 0.1 mg DPGG-modified MOF particles were dispersed in 100 μ L of 2 mg/mL lipid solution in a 60/40 (v/v) H₂O/EtOH mixture. 900 μ L H₂O was added and mixed as quickly as possible. By increasing the water concentration and with the assistance of sonication, the lipid molecules were expected to

cover the DPGG-modified MOF particles with single layer. For purification, the suspension was centrifuged (10 min, 20000 rpm), redispersed in 1 mL H₂O and again centrifuged. Finally the nanoparticles were redispersed in 100 μL H₂O.

Supporting Information

Supporting Information is available from the Wiley Online Library or from the author.

Acknowledgements

This work was supported by the U.S. DOE Office of Science, Divisions of Catalysis and Materials Science and Engineering, the Air Force Office of Scientific Research grant FA 9550-1-14-066, and the Sandia National Laboratories Lab-Directed Research and Development (LDRD) Program. We also thank Prof. Dr. Frank Caruso in the University of Melbourne for useful discussions. Sandia National Laboratories is a multimission laboratory managed and operated by National Technology and Engineering Solutions of Sandia, LLC., a wholly owned subsidiary of Honeywell International, Inc., for the U.S. Department of Energy's National Nuclear Security Administration under contract DE-NA-0003525.

Received: ((will be filled in by the editorial staff))

Revised: ((will be filled in by the editorial staff))

Published online: ((will be filled in by the editorial staff))

- [1]. (a) Furukawa, H.; Cordova, K. E.; O'Keeffe, M.; Yaghi, O. M. *Science* **2013**, *341*, 1230444; (b) Wang, C.; Liu, D.; Lin, W. *J. Am. Chem. Soc.* **2013**, *135*, 13222; (c) Bétard, A.; Fischer, R. A. *Chem. Rev.* **2012**, *112*, 1055; (d) Cohen, S. M. *Chem. Rev.* **2012**, *112*, 970; (e) Stock, N.; Biswas, S. *Chem. Rev.* **2012**, *112*, 933; (f) Murray, L. J.; Dincă, M.; Long, J. R. *Chem. Soc. Rev.* **2009**, *38*, 1294; (g) Li, J.; Sculley, J.; Zhou, H. *Chem. Rev.* **2012**, *112*, 869; (h) Ma, L.; Abney, C.; Lin, W. *Chem. Soc. Rev.* **2009**, *38*, 1248; (i) Farha, O. K.; Hupp, J. T. *Acc. Chem. Res.* **2010**, *43*, 1166.

- [2]. (a) Wang, Z.; Cohen, S. M. *Chem. Soc. Rev.*, **2009**, *38*, 1315; (b) Deria, P.; Mondloch, J. E.; Karagiari, O.; Bury, W.; Hupp, J. T.; Farha, O. K. *Chem. Soc. Rev.*, **2014**, *43*, 5896; (c) Cohen, S. M. *Chem. Rev.*, **2012**, *112*, 970.
- [3]. (a) Wang, S.; Morris, W. M.; Liu, Y.; McGuirk, M.; Zhou, Y.; Hupp, J. T.; Farha, O. K.; Mirkin, C. A. *Angew. Chem. Int. Ed.* **2015**, *54*, 14738; (b) Kondo, M.; Furukawa, S.; Hirai, K.; Kitagawa, S. *Angew. Chem. Int. Ed.* **2010**, *49*, 5327; (c) McGuire, C. V.; Forgan, R. S. *Chem. Commun.*, **2015**, *51*, 5199-5217; (d) Liu, B.; Ma, M.; Zacher, D.; Bétard, A.; Yuseenko, K.; Metzler-Nolte, N.; Wöll, C.; Fischer, R. A. *J. Am. Chem. Soc.* **2011**, *133*, 1734; (e) Jung, S.; Kim, Y.; Kim, S.-J.; Kwon, T.-H.; Huh, S.; Park, S. *Chem. Commun.* **2011**, *47*, 2904.
- [4]. (a) Nguyen, J. G.; Cohen, S. M. *J. Am. Chem. Soc.* **2010**, *132*, 4560; (b) Yang, J.; Grzech, A.; Mulder, F. M.; Dingemans, T. J. *Chem. Commun.*, **2011**, *47*, 5244.
- [5]. (a) Gadzikwa, T.; Farha, O. K.; Malliakas, C. D.; Kanatzidis, M. G.; Hupp, J. T.; Nguyen, S. T. *J. Am. Chem. Soc.* **2009**, *131*, 13613; (b) Jiang, H.; Feng, D.; Liu, T.; Li, J.; Zhou, H. *J. Am. Chem. Soc.* **2012**, *134*, 14690; (c) Morris, W.; Briley, W. E.; Auyeung, E.; Cabezas, M. D.; Mirkin, C. A. *J. Am. Chem. Soc.* **2014**, *136*, 7261; (d) Gadzikwa, T.; Lu, G.; Stern, C. L.; Wilson, S. R.; Hupp, J. T.; Nguyen, S. T. *Chem. Commun.*, **2008**, 5493.
- [6]. (a) Hong, D.; Hwang, Y. K.; Serre, C.; Férey, G.; Chang, J. *Adv. Funct. Mater.* **2009**, *19*, 1537; (b) Hwang, Y. K.; Hong, D.; Chang, J.; Jhung, S. H.; Seo, Y.; Kim, J.; Vimont, A.; Daturi, M.; Serre, C.; Férey, G. *Angew. Chem. Int. Ed.* **2008**, *47*, 4144; (c) Deria, P.; Mondloch, J. E.; Tylianakis, E.; Ghosh, P.; Bury, W.; Snurr, R. Q.; Hupp, J. T.; Farha, O. K. *J. Am. Chem. Soc.* **2013**, *135*, 16801; (d) Mondloch, J. E.; Bury, W.; Fairen-Jimenez, D.; Kwon, S.; DeMarco, E. J.; Weston, M. H.; Sarjeant, A. A.; Nguyen, S. T.; Stair, P. C.; Snurr, R. Q.; Farha, O. K.; Hupp, J. T. *J. Am. Chem. Soc.* **2013**, *135*, 10294;
- [7]. (a) Evans, J. D.; Sumbly, C. J.; Doonan, C. J. *Chem. Soc. Rev.*, **2014**, *43*, 5933; (b) Li, B.; Chrzanowski, M.; Zhang, Y.; Ma, S. *Coord. Chem. Rev.*, **2016**, *307*, 106.

- [8]. Islamoglu, T.; Goswami, S.; Li, Z.; Howarth, A. J.; Farha, O. K.; Hupp, J. T. *Acc. Chem. Res.*, **2017**, *50*, 805.
- [9]. (a) Ejima, H.; Richardson, J. J.; Liang, K.; Best, J. P.; van Koevorden, M. P.; Such, G. K.; Cui, J.; Caruso, F. *Science* **2013**, *341*, 154; (b) Bentley, W. E.; Payne, G. F.; *Science* **2013**, *341*, 136; (c) Lee, H.; Dellatore, S. M.; Miller, W. M.; Messersmith, P. B. *Science*, **2007**, *318*, 426; (d) Ejima, H.; Richardson, J. J.; Caruso, F. *Nano Today* **2017**, *12*, 136.
- [10]. (a) Guo, J.; Ping, Y.; Ejima, H.; Alt, K.; Meissner, M.; Richardson, J. J.; Yan, Y.; Peter, K.; Elverfeldt, D.; Hagemeyer, C. E.; Caruso, F. *Angew. Chem. Int. Ed.* **2014**, *53*, 5546; (b) Hu, M.; Ju, Y.; Liang, K.; Suma, T.; Cui, J.; Caruso, F. *Adv. Funct. Mater.* **2016**, *26*, 5827; (c) Sileika, T. S.; Barrett, D. G.; Zhang, R.; Lau, K. H. A.; Messersmith, P. B. *Angew. Chem. Int. Ed.* **2013**, *52*, 10766; (d) Guo, J.; Tardy, B. L.; Christofferson, A. J.; Dai Y.; Ricardson, J. J.; Zhu, W.; Hu, M.; Ju. Y.; Cui, J.; Dagastine, R. R.; Yarovsky, I.; Caruso, F. *Nat. Nanotech.*, **2016**, *11*, 1105; (e) Wang, H.; Zhu, W.; Ping, Y.; Wang, C.; Gao, N.; Yin, X.; Gu, Chen, Brinker, C. J.; Li, G. *ACS Appl. Mater. Interfaces*, **2017**, *9*, 14258.
- [11]. Sindoro, M.; Yanai, N.; Jee, A.; Granick, S. *Acc. Chem. Res.*, **2014**, *47*, 459.
- [12]. Rungtaweevoranit, B.; Baek, J.; Araujo, J. R.; Archanjo, B. S.; Choi, K. M.; Yaghi, O. M.; Somorjai, G. A. *Nano Lett.*, **2016**, *16*, 7645.
- [13]. Zimpel, A.; Preiß, T.; Röder, R.; Engelke, H.; Ingrisich, M.; Peller, M.; Rädler, J. O.; Wagner, E.; Bein, T.; Lächelt, U.; Wuttke, S. *Chem. Mater.* **2016**, *28*, 3318.
- [14]. Xiong, S.; Dunphy, D. R.; Wilkinson, D. C.; Jiang, Z.; Strzalka, J.; Wang, J.; Su, Y.; Pablo, J. J.; Brinker, C. J. *Nano Lett.* **2013**, *13*, 1041.
- [15]. (a) Yanai, N.; Granick, S. *Angew. Chem. Int. Ed.* **2012**, *51*, 5638; (b) Falcaro, P.; Ricco, R.; Doherty, C. M.; Liang, K.; Hill, A. J.; Styles, M. J. *Chem. Soc. Rev.*, **2014**, *43*, 5513.
- [16]. (a) Horcajada, P.; Chalati, T.; Serre, C.; Gillet, B.; Sebrie, C.; Baati, T.; Eubank, J. F.; Heurax, D.; Clayette, P.; Kreuz, C.; Chang, J.; Hwang, Y.; Marsaud, V.; Bories, P.;

Cynober, L.; Gil, S.; Férey, G.; Couvreur, P.; Gref, R. *Nat. Mater.* **2010**, *9*, 172; (b)

Rocca, J. D.; Liu, D.; Lin, W. *Acc. Chem. Res.*, **2011**, *44*, 957.

- [17]. Durfee, P. N.; Lin, Y.; Dunphy, D. R.; Muñiz, A. J.; Butler, K. S.; Humphrey, K. R.; Lokke, A. J.; Agola, J. O.; Chou, S. S.; Chen, I.; Wharton, W.; Townson, J. L.; Willman, C. L.; Brinker, C. J. *ACS Nano*, **2016**, *10*, 8325.
- [18]. Butler, K. S.; Durfee, P. N.; Theron, C.; Ashley, C. E.; Carnes, E. C.; Brinker, C. J. *small* **2016**, *12*, 2173.

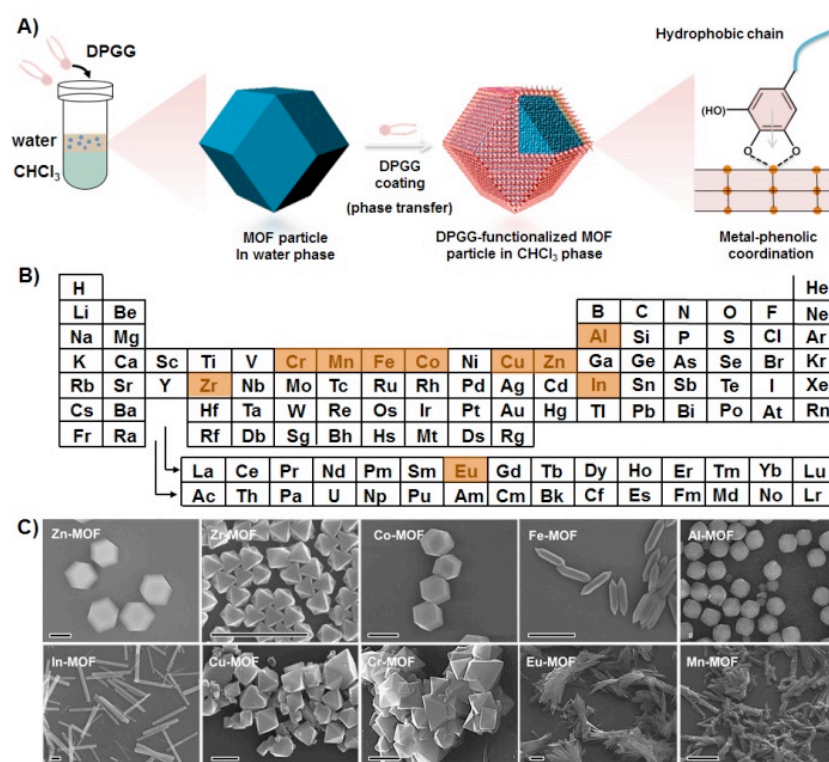


Figure 1. A) Schematic illustration of the surface functionalization of MOF particles by phase transfer reactions; B) Periodic table: metal ions highlighted in orange are used to form the related MOF particles with different shapes and porosities; C) SEM images of the DPGG-modified MOF particles; scale bar = 1 μm .

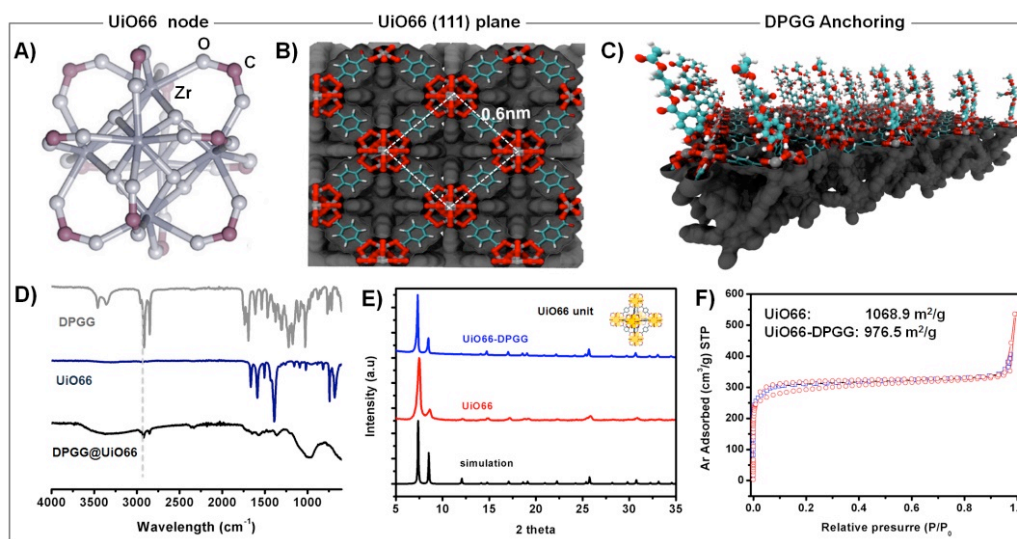


Figure 2. A) Metal cluster node of UiO66; Schematic illustration of UiO66 (111) plane without (B) and with modification of DPGG fragment (C); D) FTIR spectrum of the free DPGG molecule (top), UiO66 MOF particle (middle), and DPGG-functionalized UiO66 MOF particle (bottom); E) Wide PXRD patterns of the simulated UiO66 crystals, as-synthesized UiO66 particle, and DPGG-modified UiO66 particle; F) Ar sorption isotherms of UiO66 particles with (blue curve) and without modification of DPGG (red curve).

Table 1. Textural properties of MOF particles before and after DPGG-modification

MOF	Metal nodes	BET surface area (m ² /g)	DFT surface area (m ² /g)	DFT pore diameter, peak values (nm)	Pore volume (mL/g)
<i>UiO66</i>	Zr ₆ (μ ₃ -O) ₄ (μ ₃ -OH) ₄	1068.9	1286.1	1.22, 1.98	0.52
<i>UiO66-DPGG</i>		976.5	1169.7	1.26	0.45
<i>ZIF-8</i>	Zn ²⁺	1431.2	1603.2	1.28, 3.80	0.77
<i>ZIF-8-DPGG</i>		1280.6	1445.4	1.28, 4.00	0.74
<i>ZIF-67</i>	Co ²⁺	1495.7	1594.9	1.35, 3.80	0.75
<i>ZIF-67-DPGG</i>		1129.1	1258.8	1.30, 3.86	0.60
<i>HKUST-1</i>	Cu ^{II} ₂ (COO) ₄	1920.6	2127.1	1.33	0.79
<i>HKUST-1-DPGG</i>		1823.6	2026.3	1.35	0.75
<i>MIL-101(Cr)</i>	Cr ₃ O[O ₂ C-C ₆ H ₃ (CO ₂) ₂] ₆	2614.6	1997.5	2.43, 3.00	1.35
<i>MIL-101(Cr)-DPGG</i>		2399.8	1795.3	2.44, 3.03	1.21

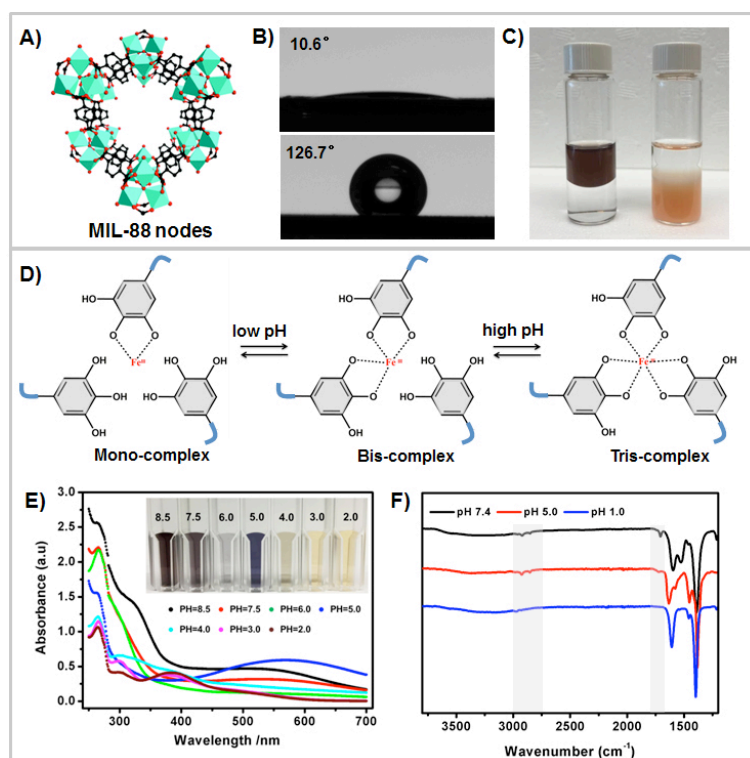


Figure 3. A) metal nodes of MIL-88A; B) contact angle images of MIL-88A MOF particles dispersed on silica slides before (top) and after DPGG-modification (bottom); C) MOF particles suspended in aqueous phase (right), and after being transferred to toluene phase after DPGG modification (left); D) Schematic illustration of the pH-dependent transition of Fe^{III}-phenolic complexation state; E) UV-Vis absorption spectra of Fe^{III}-galloyl complex in buffer with different pH. Insert is the corresponding photograph; F) FTIR of the DPGG-modified MIL-88A MOF particles after washing by buffer with different pH.

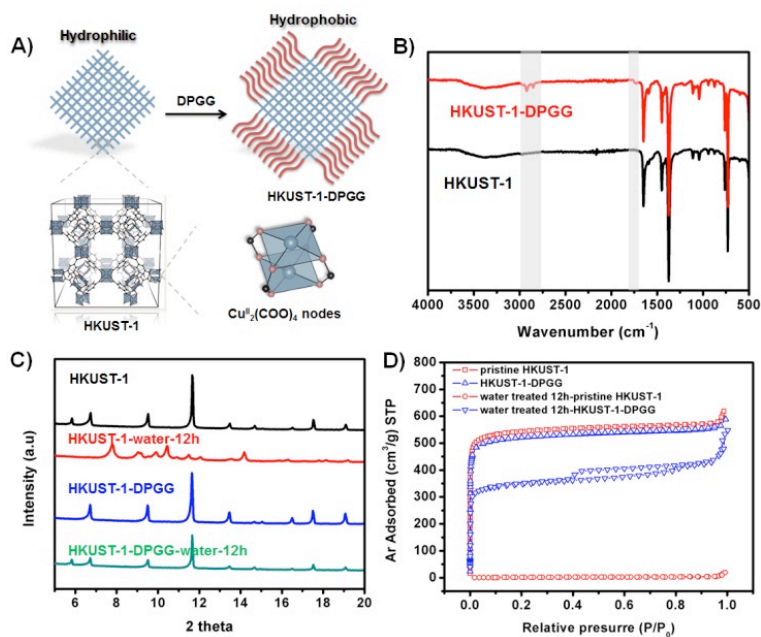


Figure 4. A) Schematic illustration of surface functionalization of HKUST-1 nanoparticles by DPGG; B) FTIR spectrum of the HKUST-1 MOF particles with and without DPGG modification; XRD (C) and Ar sorption isotherms (D) for pristine and DPGG-modified HKUST-1 nanoparticles before and after water-treatment for 12 h.

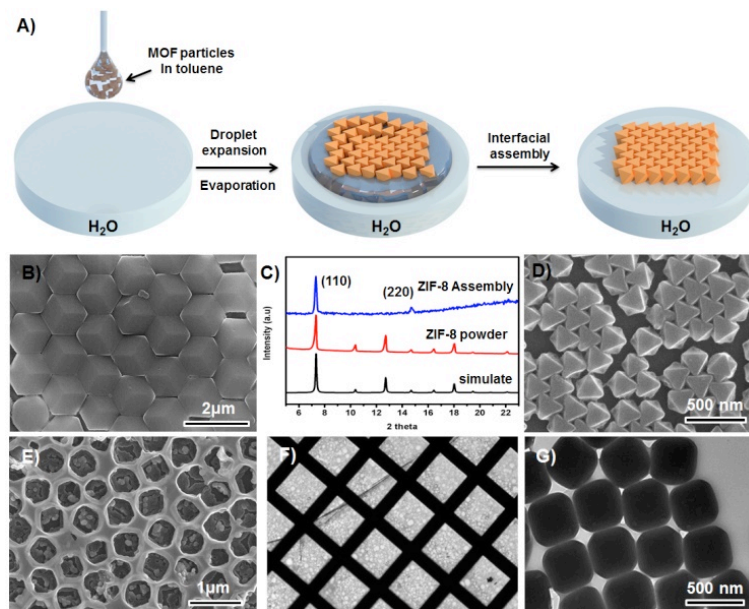


Figure 5. A) Schematic illustration of evaporation-induced interfacial assembly of DPGG-functionalized MOF particles on the air/water interface; SEM image (B) and the corresponding XRD pattern (C) of DPGG-modified ZIF-8 particles assembled on the air/water interface, followed by transfer to silica slides, showing preferential orientation; D) SEM image of interfacially assembled DPGG-modified UiO66 particles on the air/water interface; E) the assembled ZIF-8 arrays after etching by water for several days; F) Optical image of a free-standing ZIF-8/PMMA polymer film supported on a copper grid; G) TEM image of the interfacially-assembled cubic ZIF-8 particles in PMMA polymer films.

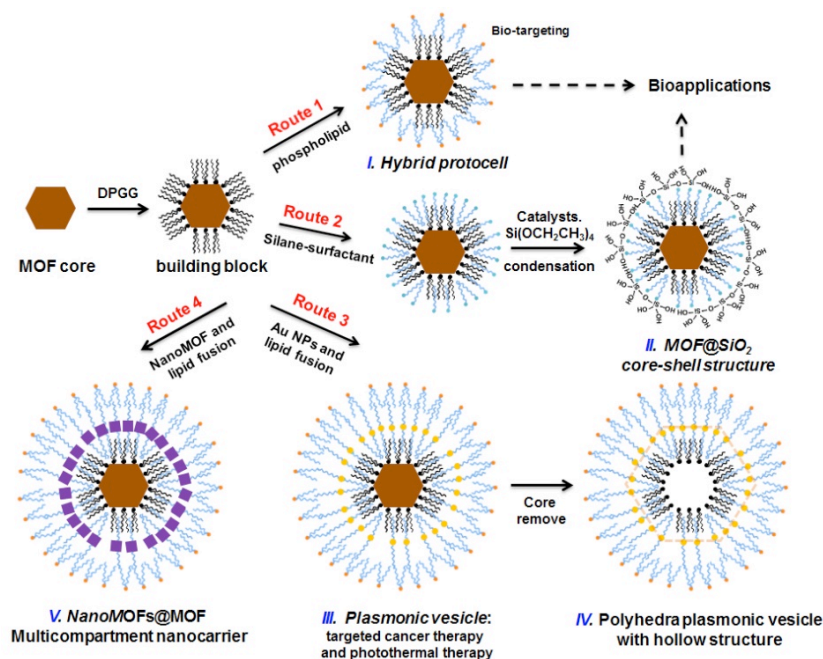


Figure 6. Schematic illustration of the sequential synthesis of various MOF-based functional nanoarchitectures: hybrid protocell (I), MOF@SiO₂ core-shell structure (II), plasmonic vesicle (III), polyhedra plasmonic vesicle with hollow structure (IV), and NanoMOF@MOF core with multicompartiment structure (V) for potential bioapplications.

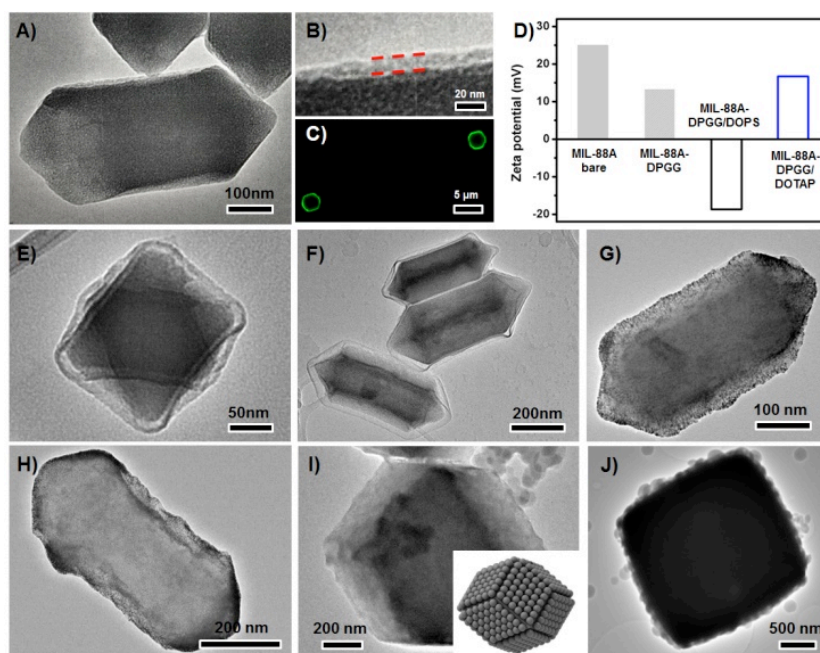


Figure 7. Cryo-TEM image of MIL-88A-DPGG-DOPS particles (A) and the related high magnification to show the hybrid lipid bilayer structure (B); (C) Fluorescence microscopy image of FTIC-labeled ZIF-8-DPGG-DOTAP microparticles; D) Zeta potential of DPGG-modified MIL-88A MOF particles after the fusion of lipid with negative or positive charge; TEM images of the particles of UiO66@SiO₂ (E), MIL-88A@SiO₂/PEG chain (F), MIL-88A-DPGG-Au NPs-DOPS (G), DPGG-Au NPs-DOPS with hollow structure (H), nanoMOFs (ZIF-8)-coated ZIF-67 (I) or mesoporous silica NPs-coated cubic ZIF-8 (J) with multicompartiment structures.

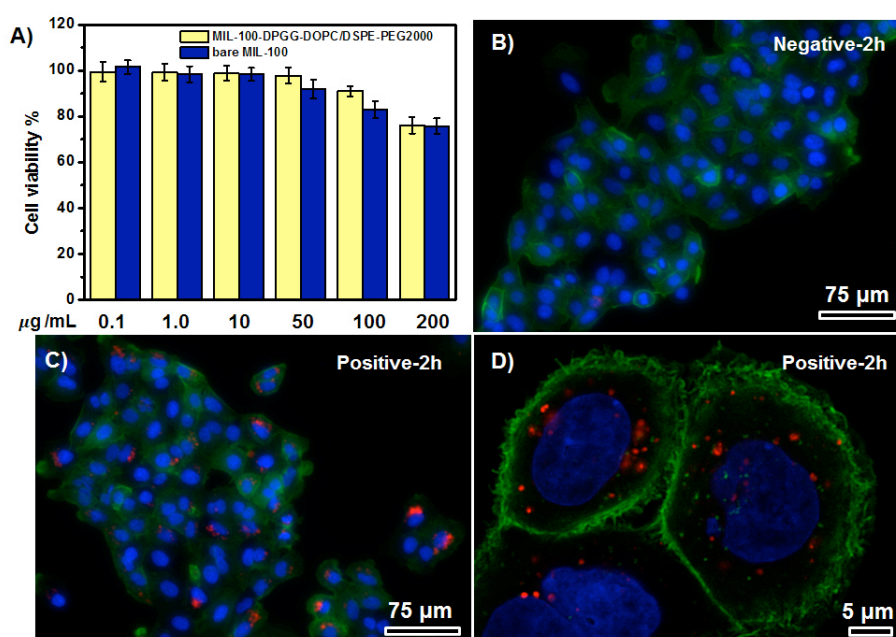


Figure 8. A) Cell viability of A549 cell measured by CellTiter-Glo® 2.0 cell viability assays for MIL-100-DPGG-DOPC/DSPE-PEG2000 and bare MIL-100 nanoparticles; Fluorescent microscopy of the internalization of MIL-100-DPGG-DOPC/DSPE-PEG2000 NPs without (B) and with (C-D) EGFR antibody functionalization by A549 cells in vitro at 2 h.

The table of contents entry

A novel strategy for the versatile functionalization of MOF external surface has been developed based on the direct coordination of lipid molecule DPGG onto metal nodes surrounding MOF surface. After DPGG functionalized, the moisture/water resistance and colloidal stability of MOFs in non-polar solvent has been greatly improved, and thus enables the related MOF self-assembly into 2D monolayer arrays via evaporation-induced interfacial assembly. By further fusion of a second functional layer onto DPGG-modified MOF cores, a series of MOF-based functional nanoarchitectures, such as MOF-based hybrid protocells, polyhedral core-shell structures, plasmonic vesicles, and multicomponent nanocarriers with target functionalities, can be easily generated for a wide range of applications.

Keyword: metal-organic framework, surface functionalization, metal-phenolic coordination, interfacial assembly, bioapplication

*Wei Zhu, Guolei Xiang, Jin Shang, Jimin Guo, Benyamin Motevalli, Paul Durfee, Jacob Ongudi Agola, Eric N. Coker, and C. Jeffrey Brinker, **

Versatile surface functionalization of metal–organic frameworks through direct metal-coordination with a phenolic lipid enables diverse applications

TOC figure

